Available online at www.sciencedirect.com
ScienceDirect
International Journal of Multiphase Flow 34 (2008) 272–282
International Journal of Multiphase Flow
www.elsevier.com/locate/ijmulflow

Disturbance growth in two-fluid channel flow: The role of capillarity

Philip Yecko *

Department of Mathematical Sciences, Montclair State University, Montclair NJ 07043, USA

Received 1 December 2006; received in revised form 26 August 2007

Abstract

This work examines the role of capillarity in the non-modal linear stability properties of three-dimensional disturbances in sheared two-layer flow of immiscible fluids of similar density. Capillarity reduces the transient growth of energy that occurs due to the non-normality of the linear stability problem according to a scaling of peak energy with $We^{1/2}$ over a wide range of Weber number, viscosity ratio and wavenumber. More importantly, the participation of capillary modes in non-modal growth leads to oscillatory energy growth and to larger disturbance growth *rates*, features that are confirmed by computing the numerical range and numerical abscissa of the non-normal disturbance evolution operator. Examination of energy components and disturbance structure reveals that early rapid growth and subsequent oscillations are due to the coupling of streamwise vortices – the two-fluid analog of lift-up – to the displaced interface.

PACS: 47.60.+i; 47.20.Ma; 47.11.Kb

Keywords: Two-fluid flow; Viscosity-stratified flow; Linear stability; Non-normal stability; Interfacial tension

1. Introduction

Layered channel flow of immiscible fluids is found in a broad range of applications, most notably in the coating and petroleum industries, and is the subject of many theoretical, experimental and simulation studies. Theoretical approaches often consider the stability of a basic flow to normal mode type disturbances, although in recent years the focus of flow stability study has shifted to also consider the transient growth of disturbances resulting from the non-normality of the system of equations that describes the evolution of linearized disturbances.

This work extends the two-fluid transient growth studies made by South and Hooper (1999) and van Noorden et al. (1998) by considering three-dimensional disturbances. Traditional eigenvalue (asymptotic) instability is not of central concern here; extensive studies of this kind can be found in, e.g., Renardy (1987), Yiantsios and Higgins (1988) or Hooper (1989) and references therein. The main results of linear eigenvalue theory can be briefly summarized: two-fluid flows involving a jump in viscosity exhibit a longwave instability first elucidated by Yih (1967). This mode is a generalization of a Kelvin–Helmholtz (KH) instability and its mechanism of growth is inviscid. Because the amplitude of this mode's eigenfunction is concentrated near the interface, Yih called this an *interfacial mode*. A different, viscous-inertial instability mechanism has been found in a slightly different flow context by Hooper and Boyd (1983) and described by Hinch (1984), occurring primarily for short waves. Both of the instabilities described above are found in two-layer Couette flow. Two-layer Poiseuille flow supports also a Tollmien–Schlichting (TS) or shear type instability mechanism, closely resembling the modes of ordinary single fluid Poiseuille flow. The stability properties at intermediate wavelengths are complicated by mode crossings, the nature of the least stable modes depending strongly on the depth, density and viscosity ratios. Numerical stability studies at intermediate wavelengths can be found in Hooper (1989) and in Yiantsios and Higgins

* Tel.: +1 973 655 5184.
E-mail address: philip.yecko@montclair.edu

0301-9322/$ - see front matter © 2007 Elsevier Ltd. All rights reserved.
doi:10.1016/j.ijmultiphaseflow.2007.09.005

(1988), where it is shown that interfacial tension stabilizes short wave disturbances.

This work studies the energy growth of disturbances in planar shear flow of two immiscible fluids, focusing on the maximum growth at intermediate times and the maximum initial growth rates. The fluids are superposed, separated by an interface on which there is constant interfacial tension σ. Flow parameters are chosen to roughly correspond to the experimental conditions of Kao and Park (1972), henceforth KP. The purpose here is to show the role of interfacial tension in the non-normal growth of disturbance energy for sheared fluids of similar densities at moderate Reynolds number.

2. Governing equations

The flow of interest is parallel channel flow of two immiscible fluids having different densities, ρ_1 and ρ_2 and different viscosities, μ_1 and μ_2, found in two layers of depths L_1 and L_2, as depicted in Fig. 1. A steady solution of the Navier–Stokes equations within the channel is obtained by solving in each layer and matching the stress on the interface, assumed flat, giving the following expression, borrowing the notation used by Hooper (1989):

$$U_1(y) = A_1 y^2 + a_1 y + 1, \quad -1 < y < 0, \tag{1}$$

$$U_2(y) = A_2 y^2 + a_2 y + 1, \quad 0 < y < n. \tag{2}$$

The flow has been scaled, introducing the parameters $n := L_2/L_1$ and $m := \mu_2/\mu_1$ for the layer depth and viscosity ratios, respectively, and $U_0 := U(0) = 1$ and $U_n := U(n)/U_0$ for the interface and upper wall velocities, respectively. The constants in Eq. (2) expressed in these terms are:

$$A_1 = \frac{-(m+n) + mU_n}{n(n+1)}; \quad A_2 = \frac{A_1}{m}, \tag{3}$$

$$a_1 = \frac{n^2 - m + mU_n}{n(n+1)}; \quad a_2 = \frac{a_1}{m}. \tag{4}$$

In this work only the pressure driven fixed walls case is considered, giving the two-fluid Poiseuille flow corresponding to $U_n = 0$.

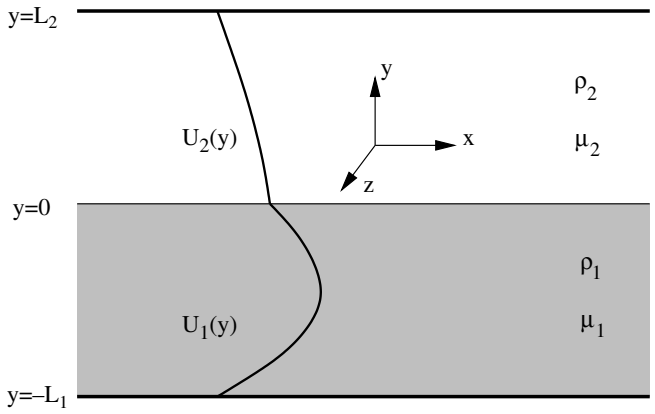

Fig. 1. Sketch of the flow configuration.

This base state is perturbed by adding an infinitesimal disturbance of the form:

$$(\mathbf{u_j}, p_j) = (\hat{\mathbf{u}}_\mathbf{j}(y,t), \hat{p}_j(y,t))\mathrm{e}^{\mathrm{i}(\alpha x + \beta z)}, \tag{5}$$

where $\mathbf{u} = (u, v, w)$, p is pressure and the subscript $j = 1, 2$ identifies the layer. The linear equations that govern the behavior of these perturbations can instead be written in terms of the normal velocity $\hat{v}_j$ and normal vorticity $\hat{\eta}_j = \mathrm{i}\beta\hat{u}_j - \mathrm{i}\alpha\hat{w}_j$:

$$\frac{\partial}{\partial t}(D^2 - k^2)\hat{v}_j + \mathrm{i}\alpha U_j(D^2 - k^2)\hat{v}_j - \mathrm{i}\alpha D^2 U_j \hat{v}_j - \frac{1}{Re_j}(D^2 - k^2)^2\hat{v}_j = 0, \tag{6}$$

$$\frac{\partial}{\partial t}\hat{\eta}_j + \mathrm{i}\alpha U_j\hat{\eta}_j + \mathrm{i}\beta D U_j \hat{v}_j - \frac{1}{Re_j}(D^2 - k^2)\hat{\eta}_j = 0, \tag{7}$$

where $k^2 = \alpha^2 + \beta^2$, $D = \mathrm{d}/\mathrm{d}y$, and boundary conditions: $\hat{v}_j = D\hat{v}_j = \hat{\eta}_j = 0$ hold on $y = -1, n$. Both layer Reynolds numbers are based on the interface velocity: $Re_j = \frac{\rho_j U_0 L_j}{\mu_j}$. Note that $Re_2 = \frac{mr}{m} Re_1$ upon defining the density ratio parameter: $r := \rho_2/\rho_1$.

A scalar interface displacement f can be defined from the kinematic condition

$$\frac{\mathrm{d}f}{\mathrm{d}t} = (\partial_t + \mathrm{i}\alpha U_j)f = \hat{v}_j \quad \text{on } y = 0. \tag{8}$$

On the interface, $y = 0$, the normal velocity v_j, the streamwise velocity $u_j = \mathrm{i}k^{-2}(\alpha D v_j - \beta\eta_j)$, and the spanwise velocity $w_j = \mathrm{i}k^{-2}(\beta D v_j + \alpha\eta_j)$ must satisfy, respectively, the following matching conditions:

$$v_2 = v_1, \tag{9}$$

$$(Dv_2 - Dv_1) - \beta(\eta_2 - \eta_1) = \mathrm{i}k^2(DU_2 - DU_1)f, \tag{10}$$

$$\beta(Dv_1 - Dv_2) = \alpha(\eta_2 - \eta_1). \tag{11}$$

Similarly, at $y = 0$ the tangential stress components τ_{xy} and τ_{yz} must satisfy:

$$m[\alpha(D^2 + k^2)v_2 - \beta D\eta_2 - \mathrm{i}k^2 D^2 U_2 f] = \alpha(D^2 + k^2)v_1 - \beta D\eta_1 - \mathrm{i}k^2 D^2 U_1 f, \tag{12}$$

$$m[\beta(D^2 + k^2)v_2 + \alpha D\eta_2] = \beta(D^2 + k^2)v_L + \alpha D\eta_1, \tag{13}$$

while the normal stress τ_{yy} condition is

$$r(\partial_t Dv_2 + \alpha DU_2 v_2) - (\partial_t v_1 + \alpha DU_1 v_1) + \frac{m(D^3 v_2 - 3k^2 Dv_2)}{\mathrm{i}Re_1} - \frac{(D^3 v_1 - 3k^2 Dv_1)}{\mathrm{i}Re_1} = -\frac{k^4}{\mathrm{i}We} f. \tag{14}$$

In (14) the Weber number also appears, defined as $We = \rho_1 U_0^2 L_1/\sigma$. No Froude number is introduced since buoyancy effects are neglected.

The above system (6)–(14) can be considered in operator form

$$\frac{\partial \mathbf{q}}{\partial t} = \mathbf{A}\mathbf{q}, \tag{15}$$

an abstract Cauchy problem with solution

$$\mathbf{q}(t) = \mathbf{q}(0)\mathrm{e}^{t\mathbf{A}}, \tag{16}$$

where $\mathbf{q}(0)$ is an initial disturbance and $\{e^{t\mathbf{A}}\}$ is a semigroup.

3. Mathematical background

Energy provides a natural disturbance measure, allowing an energy norm to be defined:

$$\|\mathbf{q}\|_E^2 = \frac{1}{2k^2}\left[\int_{-1}^{0}(|Dv_1|^2 + k^2|v_1|^2 + |\eta_1|^2)\,dy + r\int_0^n (|Dv_2|^2 + k^2|v_2|^2 + |\eta_2|^2)\,dy\right] + \frac{k^2|f|^2}{We}, \quad (17)$$

where the ultimate term characterizes the contribution of interfacial capillary energy.

The growth of a disturbance is most effectively measured by computing $\|e^{t\mathbf{A}}\|_E$ where the norm now denotes the operator norm induced by the (vector) norm of (17). The stability of the base flow will be examined by analyzing the behavior of $\|e^{t\mathbf{A}}\|_E$ as a function of t in the initial, transient and asymptotic periods – that is in the limit $t \to 0^+$, t finite, and the limit $t \to \infty$ (see Trefethen and Embree, 2005 for a complementary view of these limits).

3.1. Asymptotic growth

Introducing $\mathbf{q} = \tilde{\mathbf{q}}e^{-ist}$, where $\tilde{\mathbf{q}} = (v_2(y), \eta_2(y), f, v_1(y), \eta_1(y))^T$, allows (15) to be written as an eigenvalue problem,

$$-is\tilde{\mathbf{q}} = \mathbf{A}\tilde{\mathbf{q}}. \quad (18)$$

(Alternatively, f can be eliminated using relation (9), resulting in an eigenvalue problem of different form, as found in, e.g., Hooper and Boyd (1983); Eq. (8) is superfluous in this case.) Modal instability is identified with the presence in the spectrum of $\mathbf{A}$ of at least one eigenvalue in the upper half complex plane, viz.: $\mathrm{Im}(s_j) > 0$ for some s_j. The spectrum thus determines the behavior of disturbances, and therefore the stability of the system, at large times.

To compute the eigenvalues and eigenvectors we use a code based on Chebyshev collocation to solve the matrix form of the eigenproblem; this code was presented, validated and applied to a two-phase mixing layer in Yecko et al. (2002). Briefly, the linear problem is mapped to the Chebyshev interval $[-1, 1]$ and the eigenfunctions expressed as an expansion in a finite number N of Chebyshev polynomials $T_n(y)$ with unknown expansion coefficients. The resulting matrix problem for the expansion coefficients including the boundary and matching conditions is solved using MATLAB.

3.2. Transient growth

The eigenfunctions $\tilde{\mathbf{q}}_j$ of $\mathbf{A}$ form a complete set but are not orthogonal since $\mathbf{A}$ is not normal with respect to the inner product corresponding to the energy norm, (17), allowing some disturbances to experience significant energy growth at finite times even when eigenvalues indicate asymptotic stability. To measure this transient growth, we follow the approach advanced by Schmid and Henningson (2000) and define the energy amplification function $G(t)$ as:

$$G(t) = \|e^{t\mathbf{A}}\|_E^2 = \sup_{\mathbf{q}(0)\neq 0} \frac{\|\mathbf{q}(t)\|_E^2}{\|\mathbf{q}(0)\|_E^2} \quad (19)$$

while the maximum or optimal growth is defined as $G_O = \sup_{t\geqslant 0} G(t)$, occurring at time t_O where $G_O = G(t_O)$.

In computing transient growth, an arbitrary disturbance $\mathbf{q}$ is expressed as an expansion in the eigenfunctions of $\mathbf{A}$, viz: $\mathbf{q} = \sum_{k=1}^{K} \kappa_k \mathbf{q}_k$. $G(t)$ is then computed approximately – not in the full space of $\mathbf{A}$ but in the subspace defined by the K least stable eigenfunctions. The value K is selected large enough to achieve convergence of the approximated $G(t)$ to the limit: $\lim_{K\to\infty} G(t, K)$.

In practice, computations involving the energy norm can be recast into equivalent 2-norm problems that can be solved accurately as a singular value problem using the SVD capabilities of MATLAB, as described in Reddy et al. (1993), giving both $G(t)$ and the optimal disturbance associated with G_O; additional details can also be found in Yecko and Rossi (2004).

It has been previously noted (by Renardy (1987), van Noorden et al. (1998) and South and Hooper (1999)) that when in a two-fluid flow an interfacial energy term is not present (when interfacial tension vanishes, or $We \to \infty$) the computation of $G(t)$ in the reduced subspace of the K least unstable eigenfunctions does not converge to a limit as K is increased. Several explanations have been proposed to explain the divergent character of $G(t)$. Renardy has posited (see South and Hooper, 1999 for a discussion) that the interfacial amplitude, f, is an essential part of the disturbance eigenfunction and must be included in the norm. From the point of view of an observer, displacements of the interface due to a disturbance are certainly more visible than its energy. The "h-norm" introduced in Renardy (1987) to address flows with uniform density and no interfacial tension includes a term of the form $|f|^2$ but with constant coefficient of unity (note that any non-zero coefficient provides a valid norm). South and Hooper (1999), introducing a similar "$\mathscr{M}$-norm," found that values of this coefficient much smaller than unity work well and that this coefficient ideally should include an $(m-1)$ factor to ensure that the single fluid result is recovered for the limit $m \to 1$ (see also Malik and Hooper, 2007). In this work, the limit of zero interfacial tension is not considered, although convergence is explicitly re-checked whenever $k^2/We \ll 1$.

3.3. Initial growth rate

The initial growth rates of disturbances can be derived from the numerical range, a convex set given by:

$$W(\mathbf{A}) = \{\mathbf{q}^*\mathbf{A}\mathbf{q} \quad \text{such that } \|\mathbf{q}\|_E = 1\}. \quad (20)$$

For non-normal $\mathbf{A}$, the numerical range generally exceeds the convex hull of the spectrum, extending into the upper half-plane even for asymptotically stable $\mathbf{A}$. The initial growth rate of a disturbance corresponds to the greatest excursion of the numerical range $W(\mathbf{A})$ into the upper half complex plane, or the *numerical abscissa*:

$$\omega(\mathbf{A}) = \sup_{z\in W(\mathbf{A})} \mathrm{Im}(z) = \lim_{t\to 0^+} \frac{1}{t}\log\|\mathrm{e}^{t\mathbf{A}}\|_E = \frac{\mathrm{d}}{\mathrm{d}t}\|\mathrm{e}^{t\mathbf{A}}\|_E\Big|_0 . \tag{21}$$

We compute the numerical range and abscissa directly using what has become a standard algorithm (see Horn and Johnson, 1985): consider the set of rotated matrices: $\{\mathbf{A}_\theta\} = \{\mathrm{e}^{\mathrm{i}\theta}\mathbf{A}\}$. The normalized leading eigenvector $\mathbf{p}_\theta$ of the Hermitian matrix $\frac{1}{2}(\mathbf{A}_\theta^* + \mathbf{A}_\theta)$ is used to compute $p_\theta = \mathbf{p}_\theta^*\mathbf{A}\mathbf{p}_\theta$. For $\theta = (-\pi, \pi]$, the values of p_θ trace the boundary of $W(\mathbf{A})$, allowing $\omega(\mathbf{A})$ to be found immediately from (21). A generalized form of the above algorithm by Riedel (1994) is used in practice.

4. Results

In this study, the choice of flow parameters has been guided by the experimental conditions of KP. Attention is restricted to the single density ratio, $r = 0.9$, to equal layer depths, $n = 1$ (with one exception of $n = 2$), and maintain $Re = Re_1 = 900$. The viscosity ratio, which controls the instability of the interfacial mode, is made to range in value from $m = 1$ to $m = 20$ (in KP, $m = 20$) and the Weber number is varied from $We = 1$ to $We = 750$ (in KP, We was not reported but can be deduced to range approximately from 2 to 50, assuming no contamination occurs).

4.1. Spectrum and numerical range

The behavior of the spectrum and the numerical range for two-dimensional disturbances ($\alpha = 1, \beta = 0$) is shown in Fig. 2 for two viscosity ratios and two Weber numbers. In this section the wavenumber is held fixed so that capillary eigenvalues depend only on the Weber number. The discrete spectra, shown in Fig. 2a, maintain the characteristic 'Y' shape of Poiseuille flow, but also containing Squire modes along the vertical branch. The eigenvalues shown in the figure have been validated, in the limits $r \to 1$ and $We \to \infty$, with those given in Dongarra et al. (1996), recovering agreement to 10 digits. When the viscosity contrast is weak but interfacial tension is strong ($m = 2, We = 1$), the entire spectrum falls in the lower half-plane, although the numerical range extends into the upper half-plane a distance $\omega(\mathbf{A}) = 0.25$, as shown in Fig. 2a. At larger Weber number, the leading (interfacial) mode is unstable and its eigenvalue, $s = 1.026949 + \mathrm{i}0.002006$, falls in the upper half-plane. The numerical range in this case, by contrast, extends only to $\omega(\mathbf{A}) = 0.15$. The inflation of the numerical range is a shibboleth of non-normality and is here seen to be a direct result of the properties of the capillary modes in the spectrum.

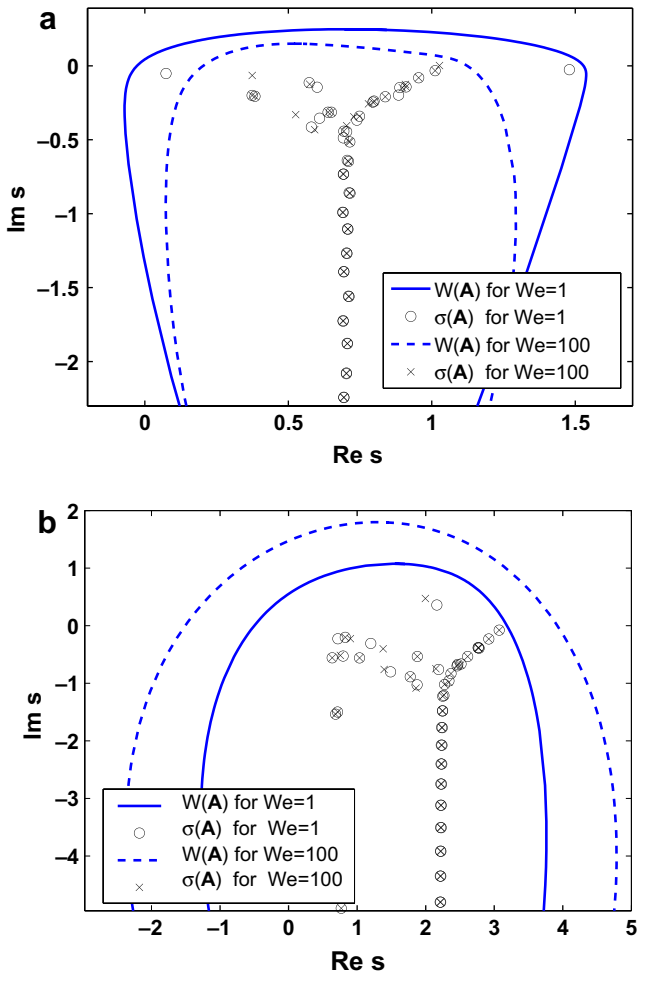

Fig. 2. Spectrum, $\sigma(\mathbf{A})$, and numerical range, $W(\mathbf{A})$, for two-dimensional disturbances: $Re = 900$, $\alpha = 1$, $\beta = 0$; (a) $m = 2$, (b) $m = 20$.

For a stronger viscosity ratio, $m = 20$, more typical of the experiments of KP, the interfacial mode for both $We = 1$ and $We = 100$ cases moves relatively far into the upper half-plane (see Fig. 2b). Due to non-normality, the numerical range extends even farther upward, giving $\omega(\mathbf{A}) = 1.1$ when $We = 1$ and $\omega(\mathbf{A}) = 1.8$ when $We = 100$. Note, however, that in contrast to the $m = 2$ case, here it is the spectral characteristics of the (unstable) interfacial mode which controls the numerical range. It is unsurprising that shear exerts a greater influence when the viscosity ratio is large.

The three-dimensional disturbances examined here are streamwise uniform, having $\alpha = 0$; such disturbances were found by Yecko and Zaleski (2005) to most strongly exhibit the non-normal behavior of this system. The spectrum of streamwise uniform modes also includes capillary waves, as shown below, facilitating the study of capillary effects. Here the wavenumber continues to be held fixed at $\beta = 1$, although in the subsequent sections β will be varied to give the largest disturbance energy amplification factor.

In each case of Fig. 3 the entire spectrum is found in the lower half-plane, and all but two modes of the spectrum

have collapsed onto the axis $\mathrm{Re}\, s = 0$. These two highly visible exceptions, found near $\mathrm{Im}\, s = 0$ with non-zero Re s, correspond to a pair of oppositely propagating weakly damped capillary waves of spanwise wavenumber $\beta = 1$. In Section 4.3, these two modes are artificially extracted to examine their contribution to energy growth. In the three-dimensional case, the numerical ranges are even more clearly expanded by the presence of these capillary modes in the spectrum. The increased numerical abscissa, $\omega(\mathbf{A})$, corresponds to increased energy growth rates at $t = 0$, as we examine in the next section. The numerical range and abscissa are larger at lower *We* (stronger capillarity) in Fig. 3a as was true in Fig. 2a, again due to the capillary component of the spectrum. In Fig. 3b (as in Fig. 2b) the viscosity ratio is increased by a factor of 10 and the numerical range instead grows as *We increases*, as a result of the decreased stability of the non-capillary modes, whose properties depend strongly on the viscosity ratio. Capillarity nevertheless enhances the energy growth rate, even in the case of Fig. 3b, as will be examined next.

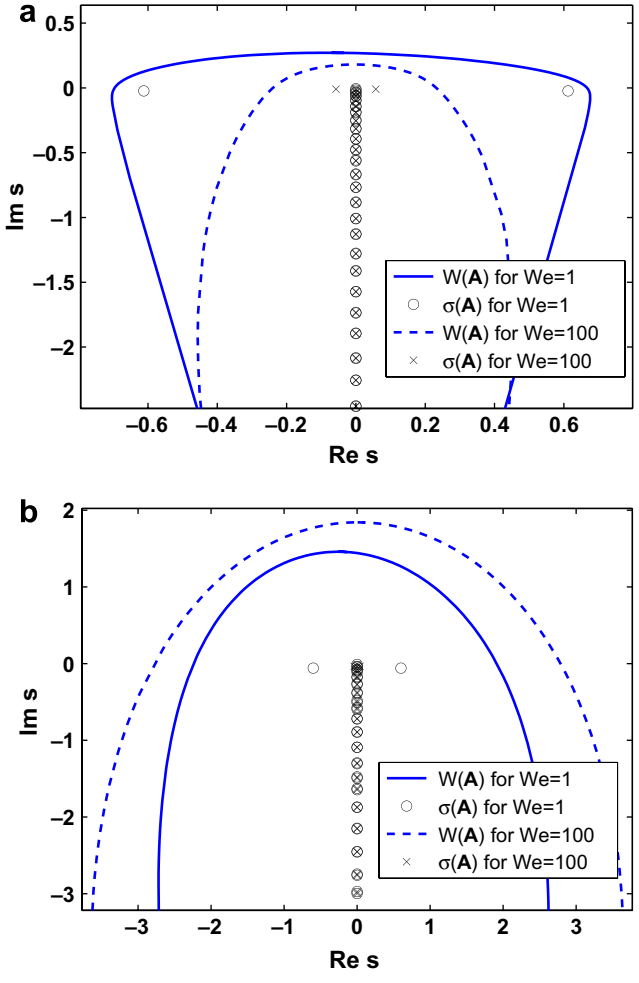

Fig. 3. Spectrum, $\sigma(\mathbf{A})$, and numerical range, $W(\mathbf{A})$, for three-dimensional disturbances: $Re = 900$, $\alpha = 0$, $\beta = 1$; (a) $m = 2$, (b) $m = 20$.

4.2. Transient energy growth rates

In the case of two-dimensional disturbances, the energy growth $G(t)$ exhibits the characteristic shape seen by South and Hooper (1999) for different flow parameters. Asymptotic instability of the interfacial mode is recovered, except for small We, as expected for two-dimensional disturbances. Any intermediate time peak in $G(t)$ is thus followed by the concurrent exponential growth. The peak growth for two-dimensional disturbances (see Fig. 4a) is not the focus of this study. Instead, we note the difference in initial growth rates at different *We* that is apparent in Fig. 4a, matching the predictions based on the numerical abscissae computed in §4.1 (see Fig. 2). The $We = 1, We = 100$ curves in Fig. 4a correspond to the same flows whose spectra and numerical ranges were depicted in Fig. 2a.

Transient energy growth of the three-dimensional disturbances first examined in Fig. 3 is computed and presented in Fig. 4b, where it is seen that increased interfacial tension reduces the transient growth peak, but again leads to larger initial growth rates. These initial growth rates correspond to the predictions based on the numerical abscissae computed in Fig. 3a. A reduction of the $G(t)$ curves is not surprising in light of the fact that interfacial tension exerts a damping influence on the modes of the spectrum.

The oscillatory behavior of the energy visible at low *We* in Fig. 4 was not seen in previous studies in which interfacial tension was neglected (South and Hooper, 1999, 2007) but "double-peak" behavior has been previously pointed out by Olsson and Henningson (1995) for watertable flow. Oscillatory growth in other non-normal systems has been linked to global instability (Coppola and DeLuca, 2006) and appears to be a generic feature of systems which support different types of modes (here capillary and shear modes) between which energy can be exchanged (Chagelishvili et al., 1997, 2005).

In Fig. 5a the effect of capillarity is examined for a wider range of *We* at the viscosity ratio $m = 20$ of the Kao and Park experiments. A monotonic increase of G_O, the peak value, with We is apparent in Fig. 5a, although at $We = 1,10$ the identification of G_O is complicated by the presence of the multiple maxima caused by oscillation in $G(t)$. The trend of G_O in Fig. 5 suggests that the first, smaller relative maximum of the $We = 1$ may not correspond to the "true" G_O value. This possibility is examined by computing the scaling relations of the peak growth G_O as a function of the *We*.

Fig. 5b presents the scaling versus Weber number of the three-dimensional disturbances (top two curves, with points) along with scalings for two-dimensional disturbances (bottom two curves, with symbols). Here the wavenumber is not fixed but has been varied to achieve the maximum growth factor $G_P := \max_\beta G_O$ where $\alpha = 0$ for three-dimensional disturbances and $G_P := \max_\alpha G_O$ where $\beta = 0$ for two-dimensional disturbances. Three-dimensional

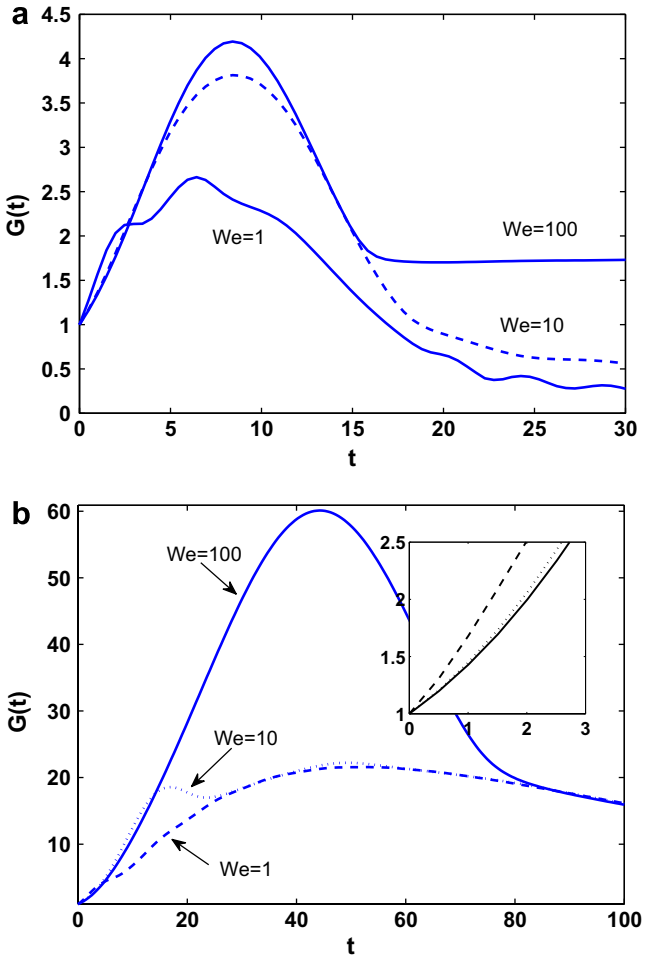

Fig. 4. Energy growth $G(t)$ at $Re = 900$, $r = 0.9$, $m = 2$ and $We = 1$, 10, 100 for two-dimensional disturbances (a) and for three-dimensional disturbances (b) inset shows early time. Weak exponential growth is visible in (a) for $We = 100$.

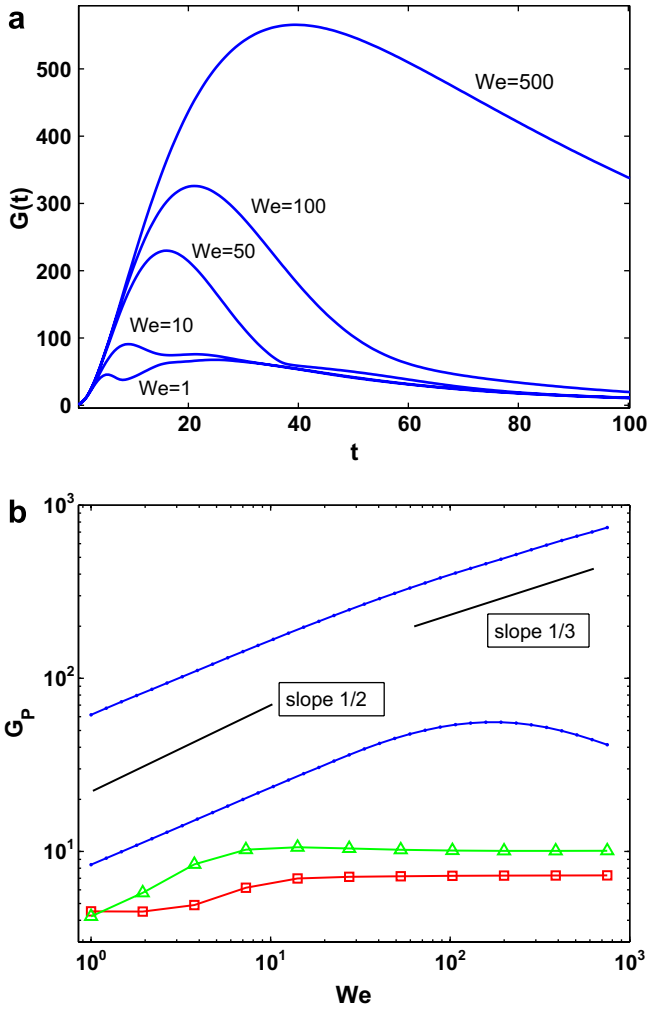

Fig. 5. (a) Energy $G(t)$ for $m = 20$, $Re = 900$, $\alpha = 0$, $\beta = 1$ at different $We = 1$, 10, 50, 100, 500; (b) scalings for 2D and 3D disturbances, see text for details.

disturbances reveal a scaling such that $G_P \propto We^{1/2}$ approximately, for $1 < We \lesssim 50$. A best fit line to the $m = 20$ curve over this range of We has slope ≈0.47. The origin of $We^{1/2}$ scaling has not been forthcoming analytically, and remains the subject of future work. Still, it seems reasonable to argue that the energy growth must deviate from an exact $We^{1/2}$ relation simply because interfacial energy is one component of total energy. Thus there should be a negligible dependence of G_O on We at large We; this is consistent with the rightmost points of Fig. 5b and much more apparent in the $m = 2$ curve. A best fit line to the $m = 20$ curve for $We \gtrsim 50$ has slope ≈0.34, as can be verified visually by comparison with the slope 1/3 line segment.

The lower curves in Fig. 5b correspond to the two-dimensional disturbance case of Fig. 4a, indicating that the peak growth is essentially independent of We for $We \gtrsim 10$. The bottom-most curve in Fig. 5b is for the same two-dimensional disturbances, but with a thinner lower layer, $n = 2$, for which increased eigenvalue stability is found (see Hooper, 1989 or Yiantsios and Higgins (1988)). Peak growth remains essentially independent of We. Yet three dimensionality alone is not what leads to We-dependent G_O, as can be seen in the counterexample of Yecko and Zaleski (2005), where identical three-dimensional disturbances (but in a matched boundary layer two-phase flow) displayed an energy peak essentially independent of We.

4.3. Direct role of capillary modes

To examine directly the role of the discrete capillary modes on $G(t)$ for streamwise uniform disturbances, the computation of energy growth has also been performed with these two modes excluded, defining the quantity $N(t)$. The result, shown in Fig. 6a, is remarkable: oscillatory behavior vanishes when capillary modes are excluded, leading to a significant change in the character of the energy growth curve. Note that the exclusion of these two capillary modes does not correspond to the elimination of capillary effects – all of the remaining modes used in the computation of $N(t)$ incorporate capillary effects, some strongly, in their eigenvalues and eigenfunctions. Equally

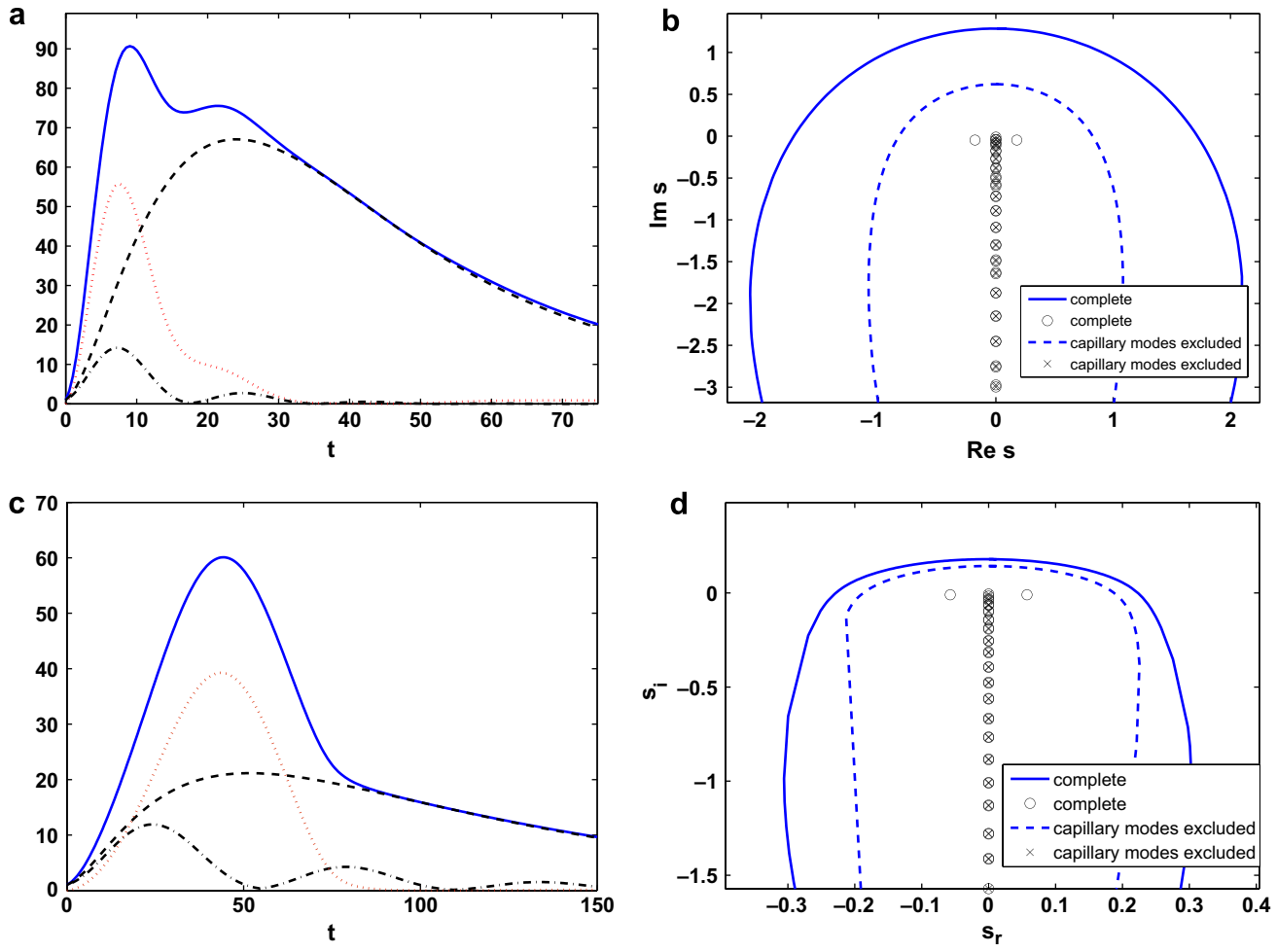

Fig. 6. Energy growth quantities $G(t)$ (solid), $N(t)$ (dashed), $C(t)$ (dash-dot), and $S(t)$ (dotted) (see text for definitions) and numerical range $W(\mathbf{A})$ for: $m = 20$ and $We = 10$ (a) and (b); and $m = 2$ and $We = 100$ (c) and (d); in all cases $Re = 900$, $\alpha = 0$, $\beta = 1$. The larger numerical abscissa effected by capillary modes is evident in (b), (d) and is reflected in the larger initial growth rate seen in $G(t)$ vs. $N(t)$ in (a), (c).

striking is the effect on the initial growth rates, which are greatly enhanced by the capillary modes, visible directly in Fig. 6a and revealed by the companion numerical ranges depicted in Fig. 6b.

At $m = 2$ and $We = 100$, shown in Fig. 6c and d, the oscillatory component of growth is less obvious, but the increase of initial growth rates effected by the capillary modes is clear, both in the energy growth (Fig. 6c) and in the numerical range and abscissa (Fig. 6d). Note that the "complete" growth curve in Fig. 6a is the same as the $We = 10$ curves in Fig. 5a. Also, the disturbance of Fig. 6c is the same as the $We = 100$ curve of Fig. 4b and will correspond to one of the optimal disturbances that will be examined in §4.4.

Also depicted in Fig. 6a and c are two other quantities related to the disturbance energy. The first is $C(t)$, the energy growth due to the two capillary modes alone. $C(t)$ is the lowest of the four plotted curves, exhibiting damped oscillations until its amplitude becomes negligible at large time. The short time growth peaks, however, indicate that these asymptotically damped capillary modes are themselves non-normal, exhibiting a transient growth. Oscillatory energy growth in a system with interfacial tension but no shear has been recently examined by Coppola and DeLuca (2006) and DeLuca and Caramiello (2001), who also linked this behavior to the peculiar properties of the spectra in non-normal systems.

The final auxiliary energy measure, identified as $S(t)$, is simply the difference: $S(t) = G(t) - N(t)$. In a normal system $S(t) = C(t)$. That $S(t) > C(t)$ for most t indicates that the capillary mode pair is not orthogonal to the complementary subspace of non-capillary modes, allowing enhanced transient growth to occur in the complete system. The physical counterpart of this property is examined next.

4.4. Optimal disturbances: Scaling and structure

To more completely examine the scaling of the energy growth first observed in §4.2, the quantity G_O is now computed over a broad range of wavenumber, Weber number and viscosity ratio. Fig. 7 displays the surface $G_O(\beta, We)$ for β in $(0, 2\pi]$ and We in $[1, 750]$ at two values of the viscosity ratio: $m = 2$ and $m = 20$. It is immediately apparent that there are two families of disturbances of greatest

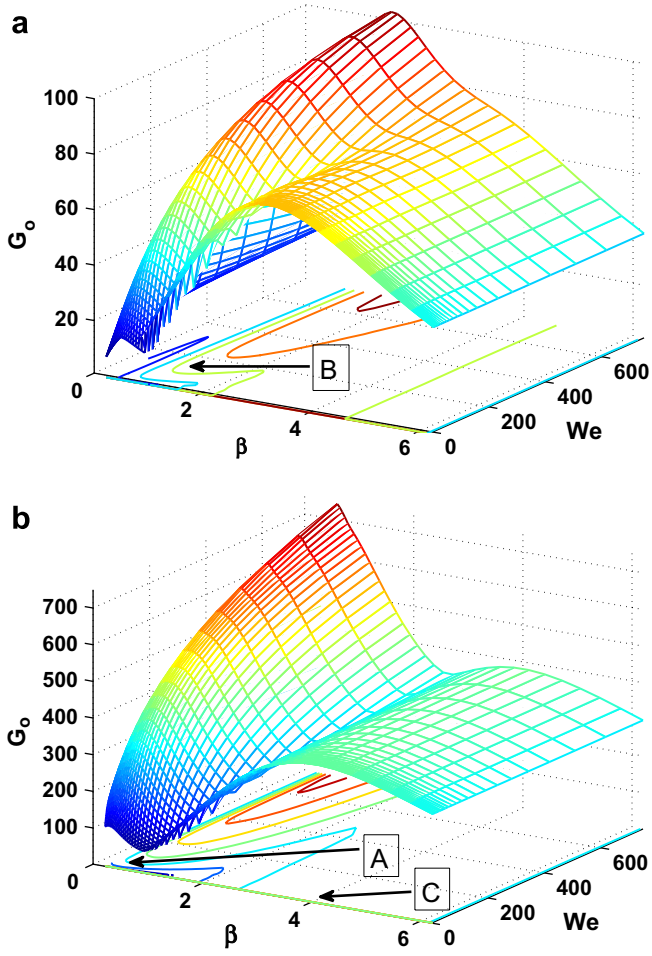

Fig. 7. Surface and projected contours of peak growth G_O as a function of wavenumber β and Weber number for $m = 2$ (a) and $m = 20$ (b); A, B, C labels refer to the optimal disturbances of Figs. 9–11.

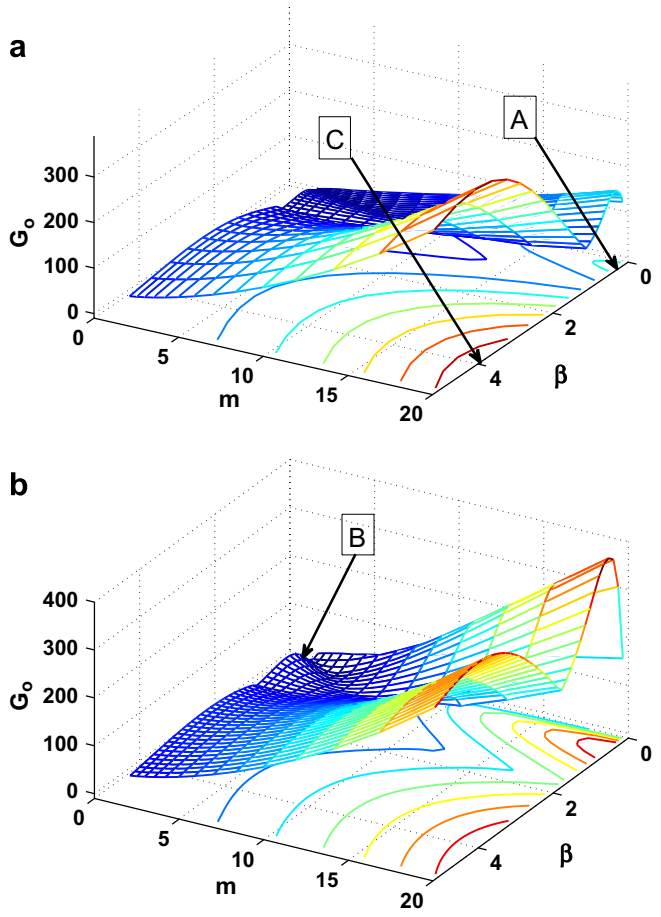

Fig. 8. Surface and projected contours of peak growth G_O as a function of wavenumber β and viscosity ratio m for $We = 10$ (a) and $We = 100$ (b); A, B, C labels refer to the optimal disturbances of Figs. 9–11.

growth (optimal disturbances): one at low wavenumber, scaling as $We^{1/2}$, and another at high wavenumber, independent of We. The wavenumber of optimal growth, β_P, of the low wavenumber disturbances also depends on We: for example, $\beta_P = 0.34$ at $We = 1$ while $\beta_P = 1.38$ at $We = 400$ (for viscosity ratio $m = 2$). The high wavenumber optimal growth occurs at $\beta_P = 3.1$ for all We at $m = 2$ (also with fixed $G_O = 72.4$) and at $\beta_P = 4$ for all We at $m = 20$ (with $G_O = 378$). The timescales over which peak growth occurs are slightly different for the high wavenumber and low wavenumber disturbances. At high wavenumber the time of peak growth, t_P, is independent of We, although its value does decrease as the viscosity ratio becomes stronger. At low wavenumber, peak growth increases weakly with We and is approximately equal to the high wavenumber time at $We = 1$.

It appears from Fig. 7 that the cases $m = 2$ and $m = 20$ differ only quantitatively, but this is not entirely the case, as can be seen in Fig. 8, where G_O is computed over the range of viscosity ratio from $m = 2$ to $m = 20$. The low wavenumber and high wavenumber peaks remain clear, but there is a shift in the β_P value of the low wavenumber peak below approximately $m = 5$, more obvious at $We = 100$ (Fig. 8b). As will be seen next, this is a consequence of a change in the disturbance flow field.

That greater growth is possible in the complete system suggests that the capillary modes both take part in and enhance the mechanism of non-normal growth. In single fluid shear, three-dimensional energy growth occurs by the so-called lift-up mechanism, in which normal velocity redistributes background shear, tapping its energy and generating normal vorticity (see Schmid and Henningson, 2000). In two-fluid shear, this mechanism is still active (see also Yecko and Zaleski, 2005) but also involves the interface displacement and therefore capillarity, and is modified by the viscosity contrast, as we show next (see also Malik and Hooper, 2007). The structure of three kinds of optimal disturbances is now examined. Each example has been chosen to be representative of a family, as identified in the peak growth maps. The disturbance flow fields are depicted in a plane normal to the flow direction, plotting (v, w) as a vector field with contours of u superimposed. The u fields at $t = 0$ fall below the contour threshold. The interface displacement f is extracted directly from the SVD solution of $G(t)$ and is depicted as a wavy

line with wavenumber β that has been normalized such that $f(t=0)=0.25$.

First, we examine the low wavenumber disturbance at $m=20$ and $We=10$, whose location is identified in Fig. 7b and Fig. 8a with the symbol 'A'. There is negligible change in this disturbance's structure as the Weber number is changed. The disturbance in this case exhibits at $t=0$ a single row of streamwise vortices whose centers are found just below the interface, as shown in Fig. 9. By $t=t_O$ the vorticity has reorganized and more closely resembles two rows of streamwise vortices. The vortices in the less viscous layer are, as expected, much stronger while the weaker upper-layer vortices are counter-rotating with respect to their lower-layer counterparts. Near the interface, the flow field surrounding these vortices has the appearance of a row of source/sink regions which are the centers of streamwise jets just below the interface, an expected lift-up type response. Energy growth has occurred mainly in the lower layer. Such disturbances qualitatively resemble those found in Malik and Hooper (2007) in the absence of interfacial tension, where they were correlated with the two leading adjoint modes of the system. A revealing feature of the nature of this type of disturbance is the favorable "in-phase" arrangement of the initially displaced interface and the initial pattern of up-welling and down-welling between vortices. This arrangement has facilitated the rapid growth of lower-layer energy by allowing very little change in the interfacial amplitude by $t=t_O$. Recall from Section 4.1 that for large m the shear destabilization of the leading interface mode eigenmodes controlled the numerical range rather than capillarity. Figs. 3b, 5a, and 6a correspond closely to the conditions of this disturbance. The second type of disturbance is also of low wavenumber type, but at $m=2$ and $We=10$, falling within the shifted G_O peak visible at small m in Fig. 8b and identified there and also in Fig. 7a with the symbol 'B'. This disturbance has $\beta_P=1$, so it also *corresponds exactly* to the cases studied in Figs. 3a, 4b and 6c. In contrast to the $m=20$ case, this disturbance begins as two rows of co-rotating streamwise vortices and evolves by $t=t_O$ into a single vortex row, with vortex centers just below the interface, as shown in Fig. 10. Also, the interface has been pushed down and

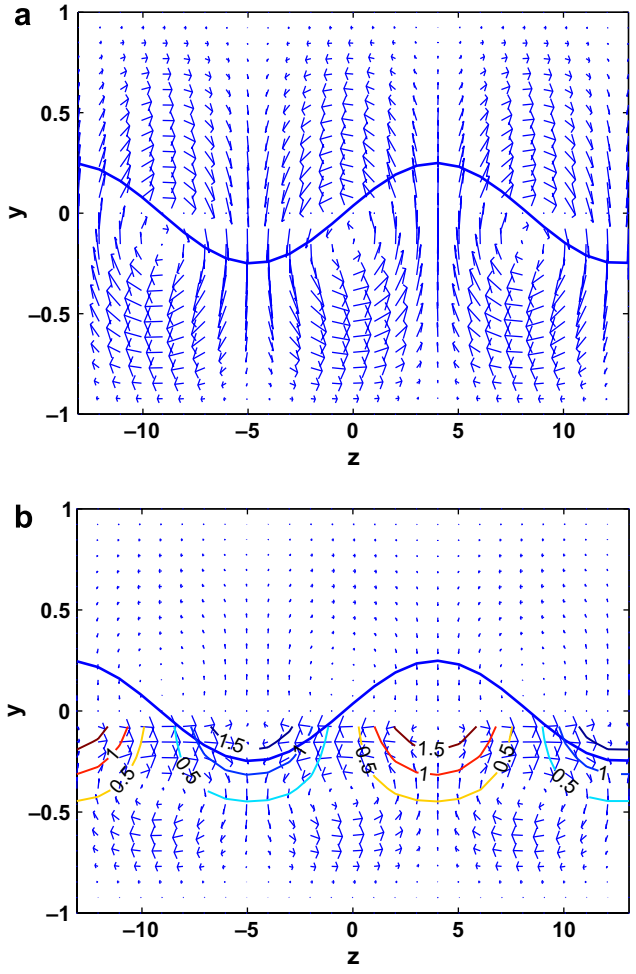

Fig. 9. Optimal disturbance A: u-contours, (v,w) vectors and interface (solid line) at $m=20$, $We=10$, $\beta_P=0.36$ shown at $t=0$ (a); and at $t=t_O$ (b). The disturbance is nearly identical for other We.

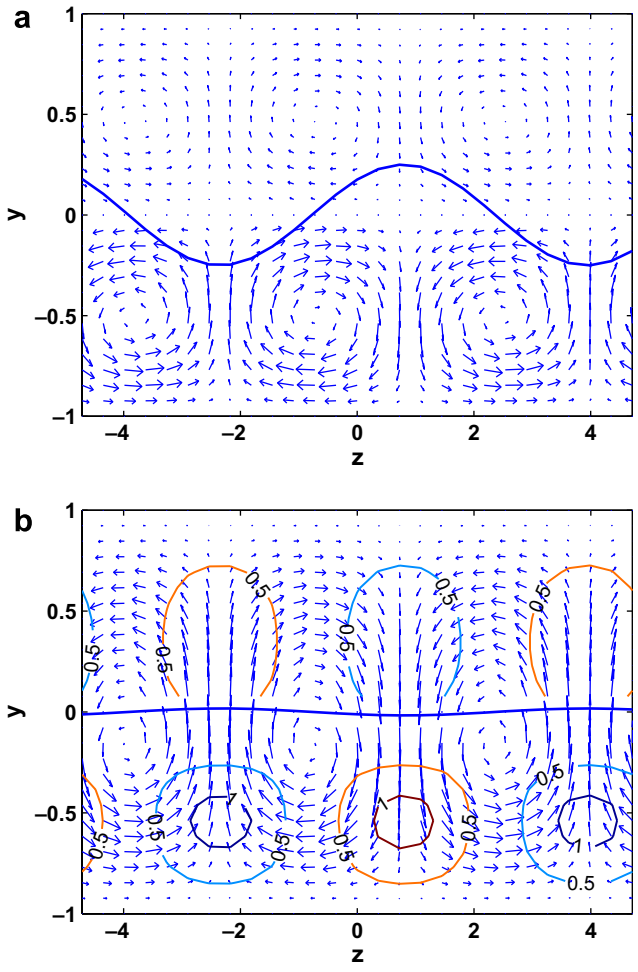

Fig. 10. Optimal disturbance B: u-contours, (v,w) vectors and interface (solid line) at $m=2$, $We=100$, $\beta_P=1$ shown at $t=0$ (a); and at $t=t_O$ (b). The disturbance is nearly identical for other We.

has slightly overshot $y = 0$ by the time of peak growth. By comparison to disturbance A and direct inspection it is clear that the interface dynamics is being assisted by the unfavorable, "out of phase" arrangement of the initial up-welling and down-welling pattern with respect to the interface wave troughs and crests. As the vorticity reduces the interface amplitude at early time, it extracts some of its energy, enhancing its initial rate of growth. Recall that at low viscosity ratio it is the capillary eigenvalues which determined the numerical range and therefore the initial growth rate.

Finally, we examine the high wavenumber, *We*-independent disturbance identified in Figs. 7b and 8a by the symbol 'C'. Because the high wavenumber peak growth factor does not depend on the Weber number, it may be assumed that capillary effects are not relevant. This assumption proves to be inaccurate, as can be concluded from the disturbance structure. Fig. 11 clearly shows that this disturbance is categorized by its rapid flattening of the interface by $t = t_O$. Disturbances of this type are thus not expected to lead to interfacial patterns. Flattening is facilitated by the unfavorable alignment of the up-welling and down-welling in the less viscous lower layer with respect to the interface troughs and crests. By $t = t_O$, lift-up has generated centers of positive and negative u velocity, including a weak row at the interface. In contrast to A or B type disturbances, the streamwise vorticity has undergone little change by t_O, although it is clear that some rearrangement has taken place between $t = 0$, when the interface amplitude is large, and $t = t_O$, when the interface is flat. That the G_O value is independent of *We* is consistent with the zero amplitude interface at t_O. Thus while capillarity has increased the initial growth rates of these disturbances, it does not contribute to the peak growth factor. A more detailed study of the combined dynamics of streamwise vortices and a deformable interface between similar density fluids is beyond the scope of this study, but analogous problems have been the focus of many investigations (see Sarpkaya, 1996 for a review, mostly in the context of free surfaces).

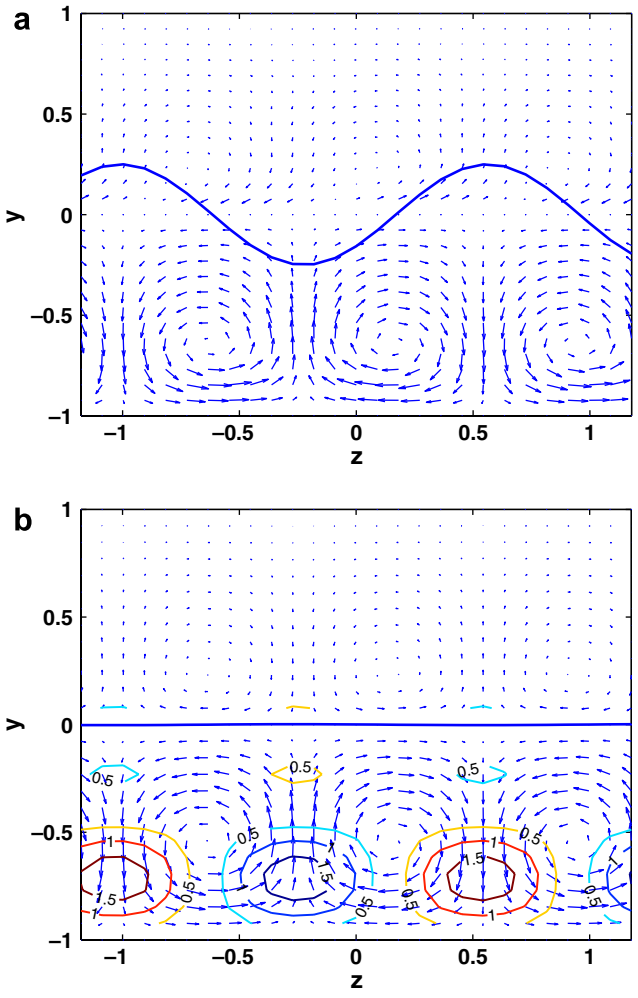

Fig. 11. High wavenumber optimal disturbance C: u-contours, (v, w) vectors and interface (solid line) at $m = 20$, $We = 10$, $\beta_P = 4$ shown at $t = 0$ (a); and at $t = t_O$ (b). The disturbance is nearly identical for other m and *We*; at $m = 2$, $\beta_P = 3.1$.

5. Conclusions

This work has examined the role of finite interfacial tension on the energy growth of three-dimensional disturbances in two-fluid channel flows. The broad effect of capillarity acts through its effect on the spectrum of eigenvalues, leading to reduced energy growth curves $G(t)$ as interfacial tension is increased and to the approximate scaling $G_O \propto We^{1/2}$ at low wavenumber. The specific effect of capillary modes however, is to facilitate a more rapid initial growth, leading to an oscillatory energy growth curve and multiple peaks at both small and large wavenumbers. These effects are found both in the direct computation of disturbance energy and in the effect of capillary modes on the spectrum. Capillary modes contribute in two ways to non-normal growth: they are themselves non-normal, exhibiting oscillatory transient growth, but they also extend the non-normality of the complete problem. Enhanced energy growth can occur because capillarity brings additional degrees of freedom to the mechanical system – specifically, capillary modes interact with the streamwise vortices of the lift-up mechanism, allowing exchange of energy between the flow disturbance and the dynamic interface. High wavenumber non-modal disturbances are able to unleash this extra energy at early times precisely because the flow associated with lift-up is arranged so as to flatten the interface, as seen directly in the disturbance flow fields. At low wavenumber, the streamwise vortices of lift-up interact in a complex way with the deforming interface, showing qualitatively different behaviors at large viscosity ratio, where shear effects dominate, than at small viscosity ratio, where capillary effects dominate. Kao and Park noticed in their experiments that most disturbed flows became quickly three-dimensional, offering also that the three dimensionality

was "enhanced by the extra degree of freedom of the interface." One may speculate that a low-dimensional system modeling the most unstable two-dimensional (interfacial) mode and the most rapidly growing three-dimensional (non-normal) disturbance would shed more light on the onset of three dimensionality. Barthelet et al. (1995) have followed a related approach, but based on two-dimensional modal disturbances, successfully explaining patterns in two-fluid Couette flow.

Finally, it is worth pointing out that when $\omega(\mathbf{A}) \leqslant 0$, the Lumer–Phillips theorem (Pazy, 1983; Trefethen and Embree, 2005) ensures no initial or subsequent growth, guaranteeing monotonic decay of energy. Thus, a nonlinear or energy stability criterion involving the capillarity should be obtainable for this problem and like similar criteria for other flow problems, is likely to be stringent.

Acknowledgements

The author thanks R. Ruben Rosales and Paolo Luchini for providing resources and hospitality; the College of Science and Mathematics (CSAM) at Montclair State University for financial support; and John G. Stevens for valuable comments.

References

Barthelet, P., Charru, F., Fabre, J., 1995. Experimental study of interfacial long waves in a two layer shear flow. J. Fluid Mech. 303, 23–53.

Chagelishvili, G.D., Tevzadze, A.G., Bodo, G., Moiseev, S.S., 1997. Linear mechanism of wave emergence from vortices in smooth shear flows. Phys. Rev. Lett. 79, 3178–3181.

Coppola, G., DeLuca, L., 2006. On transient growth oscillations in linear models. Phys. Fluids 18, 078104-4.

DeLuca, L., Caramiello, C., 2001. Temporal growth of perturbations energy in plane heterogeneous jets. AIAA Paper 2001–2704.

Dongarra, J.J., Straughan, B., Walker, D.W., 1996. Chebyshev tau-QZ algorithm methods for calculating spectra of hydrodynamics stability problems. Appl. Numer. Math. 22, 399–434.

Gogoberidze, G., Samushia, L., Chagelishvili, G.D., Lominadze, J.G., Horton, W., 2005. Surface gravity waves in deep fluid at vertical shear flows. J. Exp. Theor. Phys. 101, 169–176.

Hinch, E.J., 1984. A note on the mechanism of the instability at the interface between two shearing fluids. J. Fluid Mech. 144, 463–465.

Hooper, A.P., 1989. The stability of two superposed viscous fluids in a channel. Phys. Fluids A 1, 1133–1142.

Hooper, A.P., Boyd, W.G.C., 1983. Shear-flow instability at the interface between two viscous fluids. J. Fluid Mech. 128, 507–528.

Horn, R.A., Johnson, C.R., 1985. Matrix Analysis. Cambridge.

Kao, T.W., Park, C., 1972. Experimental investigations of the stability of channel flows. Part 2. Two-layered co-current flow in a rectangular channel. J. Fluid Mech. 52, 401–423.

Malik, S., Hooper, A.P., 2007. Three-dimensional disturbances in channel flows. Phys. Fluids 19, 052102.

Olsson, P.J., Henningson, D.S., 1995. Optimal disturbance growth in watertable flow. Stud. Appl. Math. 94, 183–210.

Pazy, A., 1983. Semigroups of Linear Operators and Applications to Partial Differential Equations. Springer.

Reddy, S.C., Schmid, P.J., Henningson, D.S., 1993. Pseudospectra of the Orr–Sommerfeld operator. SIAM J. Appl. Math. 53, 15–47.

Renardy, Y., 1987. The thin layer effect and interfacial stability in a two-layer Couette flow with similar liquids. Phys. Fluids 30, 1627–1637.

Riedel, K.S., 1994. Generalized epsilon-pseudospectra. SIAM J. Numer. Anal. 31, 1219–1225.

Sarpkaya, T., 1996. Vorticity, free surface, and surfactants. Ann. Rev. Fluid Mech. 28, 83–128.

Schmid, P.J., Henningson, D.S., 2000. Stability and Transition in Shear Flows. Springer.

South, M.J., Hooper, A.P., 1999. Linear growth in two-fluid plane Poiseuille flow. J. Fluid Mech. 381, 121–139.

Trefethen, L.N., Embree, M., 2005. Spectra and Pseudospectra: The Behavior of Nonnormal Matrices and Operators. Princeton.

van Noorden, T.L., Boomkamp, P.A.M., Knaap, M.C., Verheggen, T.M.M., 1998. Transient growth in parallel two-phase flow: Analogies and differences with single-phase flow. Phys. Fluids 10, 2099–3001.

Yecko, P., Zaleski, S., 2005. Transient growth in two-phase mixing layers. J. Fluid Mech. 17, 43–52.

Yecko, P., Rossi, M., 2004. Transient growth and instability in rotating boundary layers. Phys. Fluids 16, 2322–2335.

Yecko, P., Zaleski, S., Fullana, J.-M., 2002. Viscous modes in two-phase mixing layers. Phys. Fluids 14, 4115–4122.

Yiantsios, S.G., Higgins, B.G., 1988. Linear stability of plan Poiseuille flow of two superposed fluids. Phys. Fluids 31, 3225–3238.

Yih, C.-S., 1967. Instability due to viscosity stratification. J. Fluid Mech. 27, 337–352.